Available online at www.sciencedirect.com
ScienceDirect
Sensors and Actuators A 132 (2006) 171–181
SENSORS AND ACTUATORS A PHYSICAL
www.elsevier.com/locate/sna

A low-cost rate-grade nickel microgyroscope

Said Emre Alper*, Kanber Mithat Silay, Tayfun Akin

Middle East Technical University, Department of Electrical and Electronics Engineering, Ankara, Turkey

Received 14 September 2005; received in revised form 28 February 2006; accepted 25 March 2006
Available online 19 May 2006

Abstract

This paper presents a low-cost microgyroscope with a resolution in the rate-grade at atmospheric pressure, which is fabricated using a CMOS-compatible nickel electroforming process. Angular rate resolution of the gyroscope is increased by matching the resonance frequencies of the drive and sense modes close to each other using symmetric suspensions and electrostatic frequency tuning; whereas, undesired mechanical coupling between the two modes during matched mode operation is reduced by the fully decoupled gyro flexures. Reduced mechanical coupling results in a stable zero-rate output bias, i.e., providing excellent bias stability. The fabricated gyroscope has 18 μm-thick nickel structural layer with 2.5 μm capacitive gaps providing an aspect ratio above 7, which results in sensor capacitances about 0.5 pF. The resonance frequencies of the fabricated gyroscope are measured to be 4.09 kHz for the drive-mode and 4.33 kHz for the sense-mode, which are then matched by a tuning voltage less than 12 V dc. The gyroscope is hybrid connected to a CMOS capacitive interface circuit, and the hybrid system operation is controlled by external electronics, constructing an angular rate sensor. The gyroscope is oscillated along the drive-mode to vibration amplitude above 10 μm. The rate sensor demonstrates a noise-equivalent rate of 0.095 (°/s)/Hz$^{1/2}$ and short-term bias stability better than 0.1 °/s. The nominal scale factor of the sensor is 17.7 mV/(°/s) in a measurement range of ±100 °/s, with a full-scale nonlinearity of only 0.12%. The measurement bandwidth of the gyroscope is currently set to 30 Hz, while it can be extended beyond 100 Hz depending on the application requirements. The quality factor of the sense-mode improves by an order of magnitude at vacuum, which yields an estimated noise-equivalent rate better than 0.05 (°/s)/Hz$^{1/2}$ in a narrowed response bandwidth of 10 Hz.

Keywords: Gyroscope; Angular rate sensor; Decoupled oscillation modes; Nickel electroforming

1. Introduction

There are several applications that require reliable, low-cost, and small-size angular rate sensors, including automotive roll-over detection and industrial platform stabilization. Major performance requirements of these applications are rate-grade resolution and bias stability, both being less than 0.5 °/s [1]. These specifications are not difficult to achieve by using advanced silicon micromachining technologies such as polysilicon trench-refill [1], dissolved wafer process [2], SOI micromachining [3], silicon-on-glass micromachining [4], polysilicon surface micromachining [5], silicon bulk micromachining [6], and SOI wafer bonding to glass substrates [7]. The common features of these technologies are the high-performance at the expense of increased fabrication complexity and limited yield. In addition, monolithic integration of these fabrication processes with CMOS processes are difficult, requiring hybrid integration of the gyroscopes and CMOS electronics that increases the packaging cost. On the other hand, Analog Devices has developed CMOS-integrated inertial gyroscopes for the low-cost market [8]. These gyroscopes are fabricated with a dedicated BiCMOS manufacturing process, but the thickness of the structural polysilicon is limited to few microns. The performance of these gyroscopes is highly-improved by successful monolithic integration of the gyroscope with the high-quality readout electronics. However, the process is a dedicated process requiring high start-up and development costs. Approaches based on post-CMOS MEMS fabrication such as post-CMOS metal electroforming are attractive, since they allow to use low-cost standard CMOS foundry processes. Therefore, there are approaches in the literature to develop electroformed gyroscopes that are compatible with standard CMOS processes [9]. However, the gyroscopes developed based on electroforming have limited performances due to their low aspect ratio processes and structural limitations, resulting

* Corresponding author. Tel.: +90 312 210 4415; fax: +90 312 210 1261.
E-mail address: said@metu.edu.tr (S.E. Alper).

0924-4247/$ – see front matter © 2006 Elsevier B.V. All rights reserved.
doi:10.1016/j.sna.2006.03.031

in small sensor capacitances and drive-mode vibration amplitudes. Therefore, for low-cost rate-grade applications, it would be attractive to develop a dedicated microgyroscope structure that can be fabricated with a simple, low-cost, high-aspect-ratio, and CMOS-compatible electroforming technology.

This paper reports a new low-cost rate-grade microgyroscope fabricated with a simple and CMOS-compatible nickel electroforming process [10]. The new structure allows electrostatic tuning of resonance frequencies and large drive-mode oscillation amplitudes for enhanced sensitivity, as well as having a dedicated flexure design that minimizes mechanical cross-talk between drive and sense modes of the gyroscope due to process variations. The overall sensitivity and bias stability of the fabricated gyroscope satisfies the rate-grade performance with excellent nonlinearity in a large full-scale range and with a bandwidth sufficiently high for many applications.

2. Gyroscope structure

Fig. 1 shows the simplified three-dimensional model of the gyroscope. The proof mass is electrostatically driven into resonance along *y*-axis using linear comb drive electrodes. When the gyro frame is rotated about *z*-axis, part of the energy stored in the oscillating proof mass couples to the *x*-axis, causing the sense electrodes move along the *x*-axis. This coupled motion creates a capacitance change, which is detected using a CMOS capacitive interface circuit. The output signal from the interface circuit is then processed by external electronics providing an electrical output proportional to the applied angular rate input. Suspension flexures and anchorage of the structure is designed to restrict the motion of the movable drive and sense electrodes to 1 degree-of-freedom (DOF), whereas only the proof mass is allowed to 2 DOF motion. This configuration minimizes undesired mechanical cross-talk between the drive and sense modes. The drive-mode of the gyroscope is optimized for large amplitude and linear driving oscillations using linear comb fingers, whereas the sense-mode is optimized for increased rate sensitivity and electrostatic tuning using varying-gap type comb fingers. Finally, flexures are designed symmetric along the drive and sense modes for minimizing possible temperature-dependent drift [11].

3. Fabrication process

Fig. 2 shows the fabrication process flow that requires only three masks. The process starts with deposition and patterning of 300/3000 Å-thick evaporated Cr/Au metallization layer over a 500 μm-thick, 4-inch, Corning 7740 Pyrex glass substrate. Next, a 300/3000 Å-thick Ti/Cu seed layer is sputter-coated on the whole substrate surface. The Ti/Cu seed layer is then etched away inside the anchor and pad metallization regions, for ensuring that the nickel is electroformed on Cr/Au stack rather than on Ti/Cu stack at the structural layer formation step towards the end of the process (Fig. 2h). Otherwise, nickel structures detach from the substrate surface during long sacrificial layer etch at the final step of the process. Following the patterning of a 5.5 μm-thick negative-tone photoresist (Microposit ma-N 440) with controllable-sidewall profile, the copper sacrificial layer is electroformed from copper sulfate chemistry on the whole substrate surface except inside the anchor regions. Next, the negative-tone photoresist is stripped from the substrate surface and Shipley's SJR5740 photoresist is coated to a thickness of about 20 μm and patterned using the structural layer mask. After cleaning the surface of the underlying conductive Ti/Cu and Cr/Au seed layer regions with oxygen plasma and hardbaking the structural photoresist mold, nickel is electroformed inside the thick photoresist mold from a low-stress nickel sulphamate chemistry. Finally, the thick photoresist mold is stripped in the SVC175 photoresist stripper, and the copper sacrificial layer and the Ti/Cu seed layer are selectively etched in a mixture of 1:1:18 acetic acid (CH_3COOH), H_2O_2, and deionized water. Fabricated nickel gyroscopes are then cleaned in deionized water, rinsed in a standard acetone–isopropyl alcohol (IPA)–methanol bath, and released by drying on hotplate.

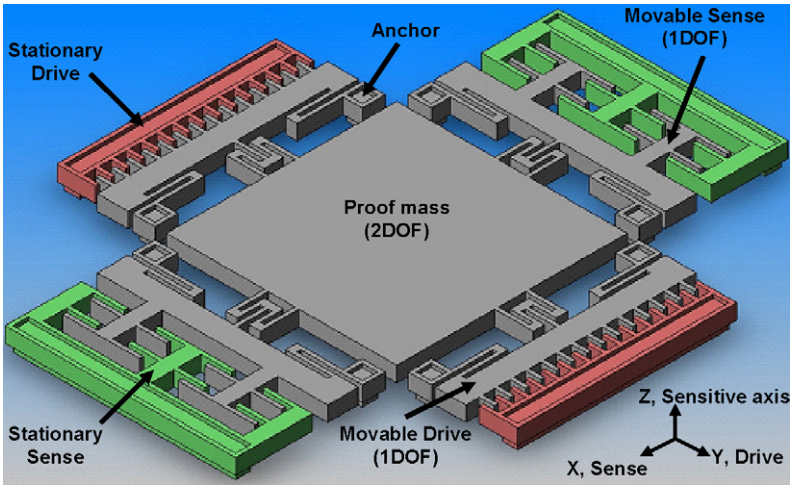

Fig. 1. Simplified three-dimensional model of the gyroscope with symmetrically-located and decoupled suspension flexures and anchorage restricting the motion of the movable drive and sense electrodes to 1 degree-of-freedom (DOF), whereas only the proof mass is allowed to 2 DOF motion. The structure has linear drive combs allowing large drive-mode vibration amplitudes, large sense capacitances with electrostatic tuning capability, and folded flexures for linear drive-mode vibrations.

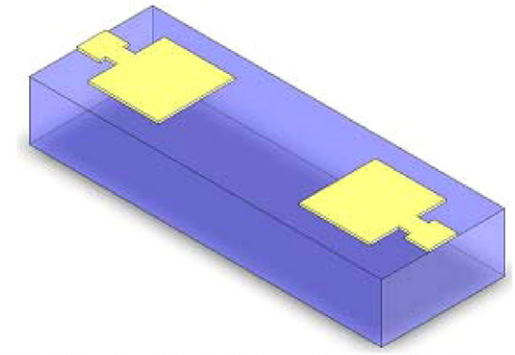

(a) Pattern Cr/Au pad metallization on a blank glass substrate

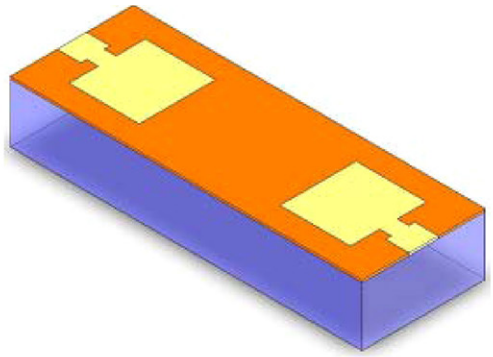

(b) Pattern Ti/Cu on the whole substrate surface as a seed layer for copper electroforming

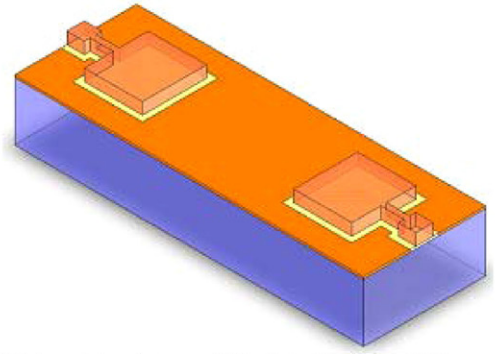

(c) Pattern photoresist as a mold for electroforming sacrificial copper

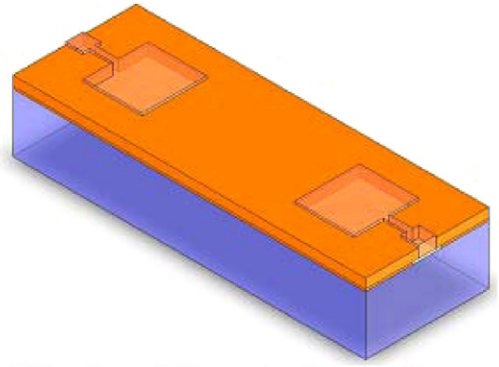

(d) Electroform sacrificial copper into photoresist mold

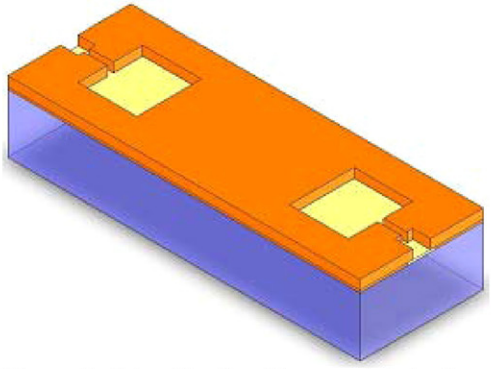

(e) Remove the photoresist mold used for copper electroforming

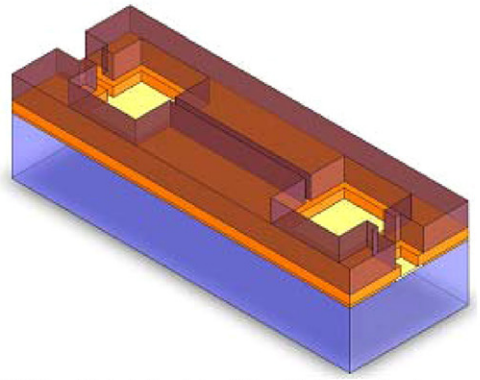

(f) Pattern thick photoresist mold for nickel electroforming

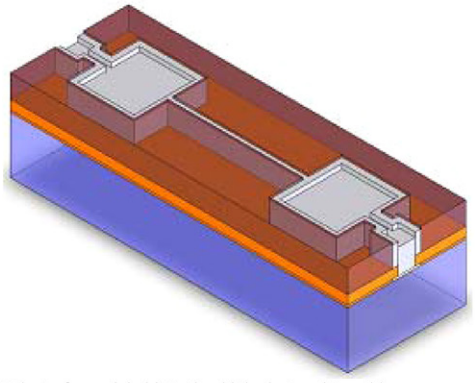

(g) Electroform nickel into the thick photoresist mold

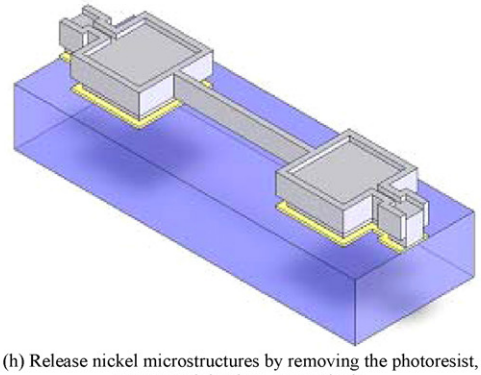

(h) Release nickel microstructures by removing the photoresist, copper, and titanium, respectively.

Fig. 2. Fabrication process flow that requires only three masks.

Table 1
Bath constituents and operating conditions for copper electroforming process

Constituent	Concentration	Parameter	Condition
Copper sulfate	220 (g/l)	Plating current type	20% dusty-cycle forward-pulse
Sulphuric acid	32 (ml/l)	Plating current density	2 (A/dm^2)
Basic brightener	4 (ml/l)	Deposition rate	0.4 (μm/min)
Leveling agent	0.4 (ml/l)	Filter agitation	Off
Wetting agent	20 (ml/l)	Anode–cathode spacing	5 (mm)
		Anode agitation freq.	3 (Hz)
		Bath temperature	25 °C

Tensile stress and surface roughness of electroformed copper sacrificial layer is reduced by optimizing the copper electroforming process. Table 1 summarizes the bath constituents and operating conditions for the developed copper electroforming process. In addition, the surface roughness, residual stress, and pitting of the electroformed nickel are improved by optimizing the operating conditions for the nickel sulphamate bath and by using an electroplating setup with agitators covered with fibrilic clothing based on a technology for reducing boundary layer thickness [12]. Table 2 summarizes the bath constituents and operating conditions for nickel electroforming process.

The overall process is CMOS-compatible with process temperatures below 120 °C and requires only three masks, a standard UV lithography equipment, and a low-cost electroplating setup. Therefore, the fabrication cost of unpackaged gyroscopes are very low with this approach. It should be mentioned that the cost of packaging contributes significantly to the overall cost of the MEMS gyroscope, especially if hermetic vacuum sealing is required. On the other hand, the start-up and development cost for the fabrication process would have an increasing importance in the near future due to the possible reduction in packaging costs with the recent advances in wafer-level encapsulation technologies. Therefore, when low-cost wafer-level packaging is considered, the cost of the packaging will be comparable to the cost of the fabrication of the unpackaged gyroscope. As a result, low-cost electroforming technologies would be attractive for high-volume low-cost sensor production with integrated electronics.

Fig. 3 shows the scanning electron microscope (SEM) photographs of the fabricated gyroscope. The gyroscope occupies an area of 2.9 mm × 2.9 mm including the bonding pads, while the overall chip area is set 3.3 mm × 3.3 mm for dicing tolerances. The movable structure is suspended 5 μm over the substrate, defined by the thickness of the copper sacrificial layer.

Fig. 4 shows the close-up SEM photographs of the varying-overlap-area type drive combs and varying-gap type sense combs. The height of the structural layer of the gyroscope is measured as 18 μm, whereas the electrostatic gap between the fabricated comb fingers is only 2.5 μm. The aspect ratio of the currently fabricated gyroscope is therefore higher than 7, which is actually the physical limit for electroforming processes using standard UV lithography for patterning a standard thick photoresist such as SJR5740.

4. Characterization and results

The drive and sense electrode capacitances of the gyroscope are measured using Agilent 4294A precision impedance analyzer as 405 fF and 455 fF, respectively, for 2.5 μm fabricated capacitive gaps. These values agree well with the design values of 352 fF and 381 fF, respectively, for the 3 μm designed-value for the capacitive gaps.

Fig. 5 shows the measurements of the drive and sense-mode resonance characteristics for the fabricated gyroscope using the Agilent 35670A dynamic signal analyzer and Karl Suss micromanipulator probe station. The resonance frequencies of the drive and sense modes of the fabricated gyroscope are measured to be matched at 4090 Hz for a dc polarization voltage of 12 V applied to the proof mass. The measured resonance frequency of the drive-mode is somewhat smaller than the designed frequency of 4678 Hz, primarily due to the fabricated beam widths being 2.75 μm instead of the 3 μm design value. The structure is designed to provide a sense-mode resonance frequency matched to the drive-mode resonance frequency at a dc voltage of 9.8 V

Table 2
Bath constituents and operating conditions for nickel electroforming process

Constituent	Concentration	Parameter	Condition
Nickel sulphamate	500 (g/l)	Plating current type	dc Current
Boric acid	30 (g/l)	Plating current density	0.4–1.1 (A/dm^2)
Nickel chloride	2 (g/l)	Deposition rate	0.4–1.1 (μm/min)
		Filter agitation	On
		Anode–cathode spacing	7.4 (mm)
		Anode agitation freq.	2.1 (Hz)
		pH of the solution	3.8–4.2
		Bath temperature	45 °C
		Anode-type	Insoluble (titanium)

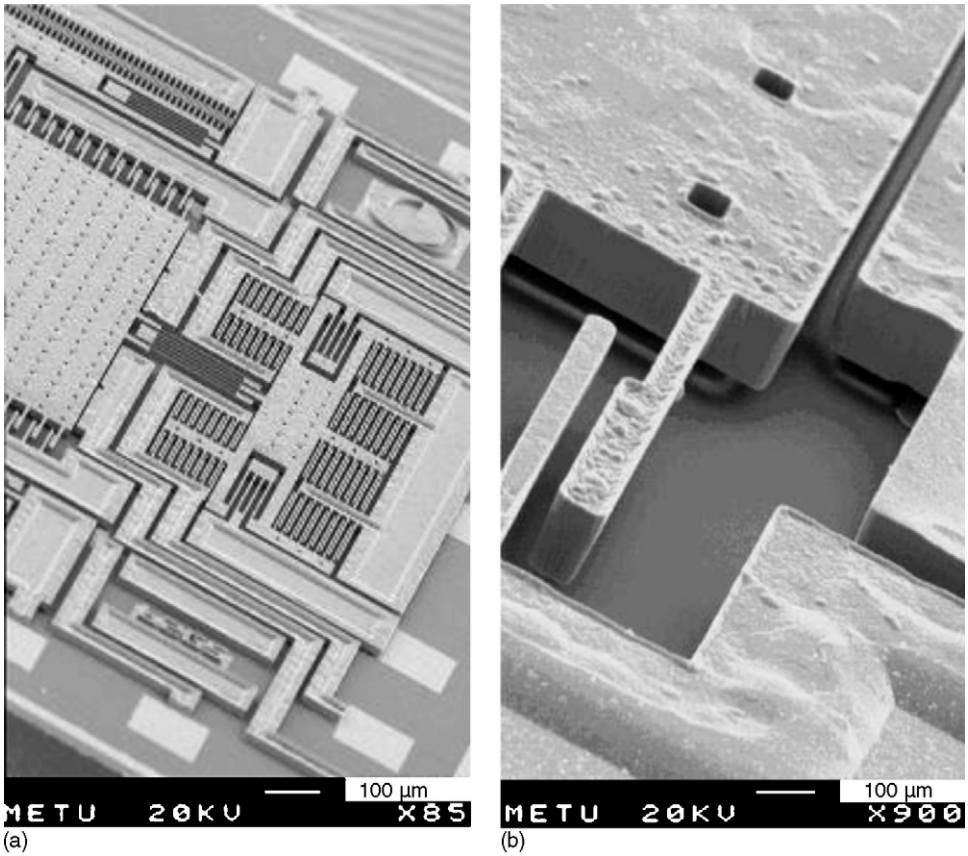

Fig. 3. The scanning electron microscope (SEM) photographs of the fabricated gyroscope. (a) The gyroscope occupies an area of 2.9 mm × 2.9 mm including the bonding pads, while the overall chip area is set 3.3 mm × 3.3 mm for dicing tolerances. (b) The movable structure is suspended 5 μm over the substrate, defined by the thickness of the copper sacrificial layer.

applied to the proof mass. In measurements, it is found out that the voltage for matching the two resonance frequencies is 12 V, which can be expected due to variations in the structural dimensions after the process compared to the designed values.

The quality factors of the nickel gyroscope for the drive and the sense modes at atmospheric pressure are then measured to be 381 and 55, respectively. The lower quality factor of the sense-mode is a result of higher air damping along the sense-mode due to the high-aspect-ratio varying-gap type sense electrodes.

The fabricated gyroscope is hybrid connected to a single-ended CMOS capacitive interface circuit, which is similar to a previously designed structure [7]. Fig. 6 shows the schematic view of the CMOS interface circuit. The capacitive interface circuit has high input-impedance in order to buffer the high-impedance sensor output. High input-impedance is achieved by minimizing the parasitic capacitance associated with the CMOS chip using bootstrapping method, whereas the parasitic capacitance associated with the gyroscope chip is already minimized due to insulating substrate. The designed capacitive interface circuit is fabricated in the XFAB 0.6 μm CMOS process and measures only 0.7 mm × 1.3 mm. Fig. 7 shows the photograph of the fabricated nickel gyroscope hybrid connected to the CMOS capacitive interface circuit inside a 40-pin DIL package.

Fig. 8 demonstrates the effective frequency tuning for the sense-mode of the gyroscope. The sense-mode resonance frequency of the gyroscope can be reduced from 4.25 kHz at 5 V dc down to 3.58 kHz at 20 V dc by negative electrostatic spring constant. The total electrostatic spring constant of the fabricated gyroscope is found to be $-(0.1016)V_{dc}^2$, where V_{dc} is the dc voltage across the varying-gap type sense electrodes. The measured electrostatic spring constant is in close agreement with the expected value of $-(0.1006)V_{dc}^2$.

Table 3 presents a comparison of the designed and the measured electrical and mechanical parameters for the fabricated nickel gyroscope. In general, the measured values agree well with the design values considering that the capacitive gap spacing and flexure beam widths are slightly different than the design values due to fabrication tolerances.

Fig. 9 shows the electronic blocks constructed using off-the-shelf components and functioning as a simple positive-feedback loop for drive-mode self-resonance excitation of the fabricated gyroscope. The loop includes the second-order model of a rate sensor, an ac coupler, a phase-shifter, and a final gain stage, and it is self-triggered while switching the power on. The second-order model of the rate sensor includes the drive-mode resonator of the gyroscope and the capacitive interface circuit hybrid-connected to the gyroscope output. The output of the capacitive interface circuit is filtered through an ac coupler, in order to remove any dc offset coming from the interface circuit. The phase-shifter generates the correct phase for electrostatic actuation to be supplied to the gyroscope input. The final gain stage is necessary to

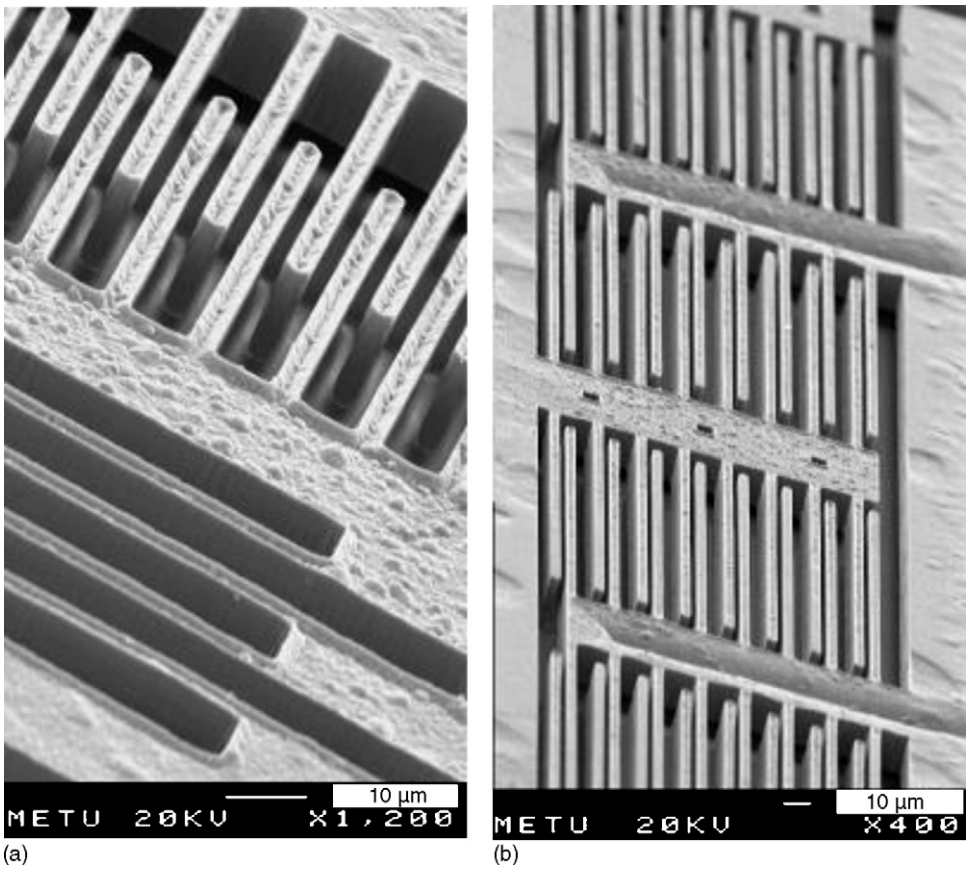

Fig. 4. Close-up SEM photographs of (a) varying-overlap-area type drive combs and (b) varying-gap type sense combs. The height of the structural layer of the gyroscope is measured as 18 µm, whereas the electrostatic gap between the fabricated comb fingers is only 2.5 µm. The aspect ratio of the currently fabricated gyroscope is therefore higher than 7.

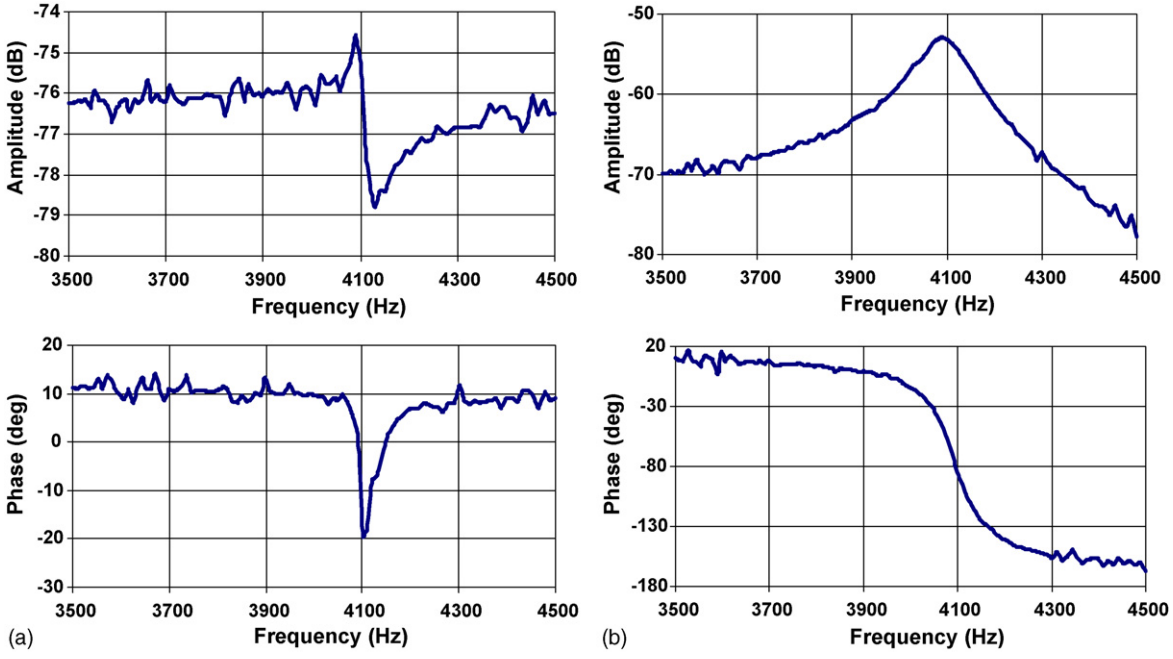

Fig. 5. The measurements of (a) drive and (b) sense-mode resonance characteristics for the fabricated gyroscope using Agilent 35670A dynamic signal analyzer and Karl Suss micromanipulator probe station.

Table 3
Comparison of the designed and the measured electrical and mechanical parameters for the fabricated nickel gyroscope

Parameter	Designed		Measured	
	Drive	Sense	Drive	Sense
Capacitive gap (μm)	3	3	2.5	2.5
Capacitive anti-gap (μm)	N/A	8	N/A	8.3
Capacitance (fF)	352	381	405	455[a]
$\partial C/\partial x$ (F/m)	8.88×10^{-9}	9.00×10^{-8}	6.15×10^{-9}	5.9×10^{-8}
$\partial^2 C/\partial x^2$ (F/m^2)	N/A	−0.1006	N/A	−0.1016
Mechanical spring constant (N/m)	146	169	111	136.6[b]
Average beam width (μm)	4	4	3.65	3.76
Mechanical resonance freq. (Hz)	4678	4823	4090	4336[c]
Parasitic capacitance (fF)	<500[d]	<500[d]	224	79
Voltage required for frequency matching (V_{dc})	N/A	9.8	N/A	12

[a] Result excludes the anti-gap capacitance, which is theoretically evaluated about 108 fF regarding the measured anti-gap of the fabricated gyroscope.
[b] Excludes the measured electrostatic spring constant.
[c] Includes only the extracted mechanical spring constant.
[d] A maximum of 0.5 pF parasitic capacitance is expected for hybrid wirebonding.

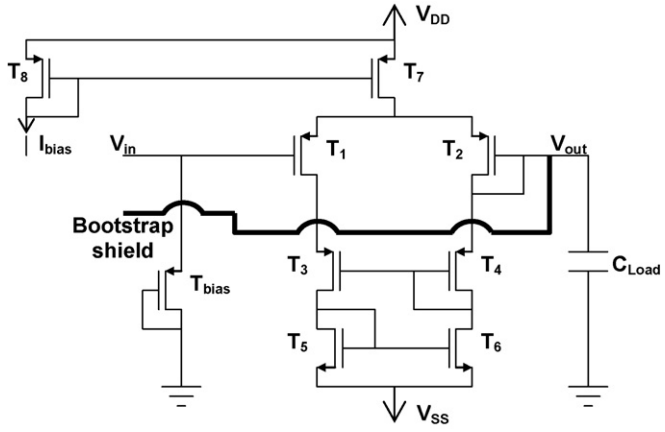

Fig. 6. The schematic view of the CMOS capacitive interface circuit.

satisfy the overall gain of the system being above unity, so as to cause an amplitude build-up as a result of positive feedback. The amplitude would be limited by the voltage swings determined by the supply voltages of the electronic components constructing the self-resonance loop. The feedback loop of Fig. 9 presents a simple method to generate self-oscillations along the drive-mode, the frequency of which is determined by the mechanical resonance frequency of the gyroscope provided that the phases of the signals are carefully controlled inside the loop. The control of the signal phase inside the loop is very important for starting the self-resonance oscillations. Table 4 provides a fast look-up reference for checking the phase of the signals for the proposed gyroscope, depending on the frequency matching and the impedance of the interface circuit. After constructing the self-oscillation loop, the drive-mode vibration amplitude of the gyroscope is set to 10 μm at resonance, limited by the linear operation range for the drive-mode flexures.

Fig. 10 shows the measured spectrum of the sense-mode output of the fabricated nickel angular rate sensor in response to a sinusoidal angular rate input of amplitude 2π °/s and frequency 10 Hz. The two side-lobes in the figure correspond to the rate outputs, separated from the quadrature signal (central peak) by a frequency equal to the frequency of the applied rate input. The mechanical sensitivity of the nickel gyroscope is measured to be 180 μV/(°/s). The estimated sense-mode displacement

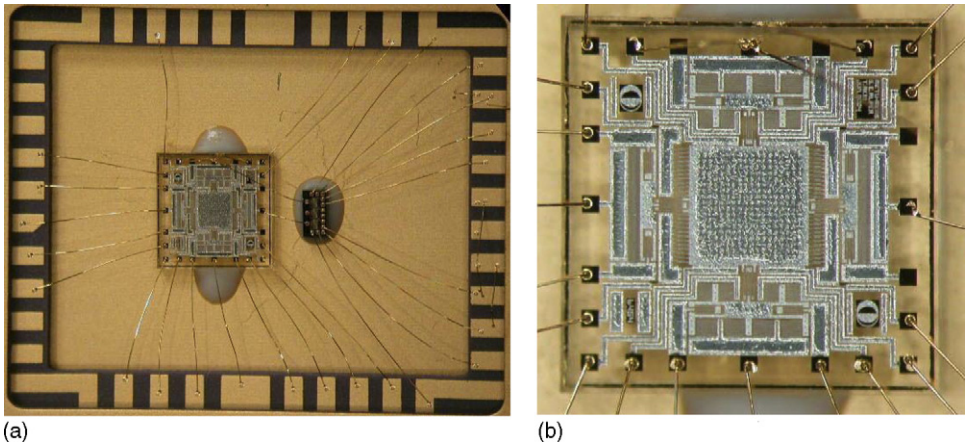

Fig. 7. (a) The photograph of the fabricated nickel gyroscope hybrid connected to the CMOS capacitive interface circuit inside a 40-pin DIL package. (b) Close-up view of the gyroscope chip.

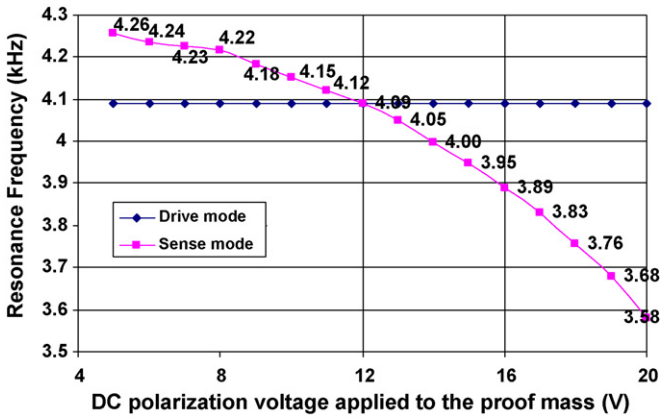

Fig. 8. Effective frequency tuning for the sense-mode of the fabricated nickel gyroscope. Sense-mode resonance frequency of the gyroscope can be reduced from 4.25 kHz at 5 V dc down to 3.58 kHz at 20 V dc by negative electrostatic spring constant.

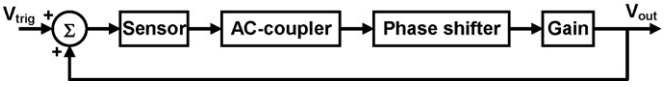

Fig. 9. The electronic blocks used for constructing the simple positive-feedback loop for drive-mode self-resonance excitation of the fabricated gyroscope.

is 6.1 Å/(°/s), corresponding to a generated output voltage of 280 μV for 1 °/s rate input, which is higher than the measured value of 180 μV. However, the estimated value assumes perfect matching of the resonance frequencies of the drive and sense modes, whereas the two modes are tuned within a matching tolerance of 40 Hz, which is typical for manual frequency tuning where there is no electronic feedback control. The quadrature signal at the sense-mode output is 42 mV corresponding to about 230 °/s, which is suppressed by phase-sensitive demodulation of the sense-mode output. Finally, the rms noise floor of the gyroscope is found to be 20 μV/Hz$^{1/2}$. The mechanical-thermal noise of the nickel gyroscope is estimated to be smaller than 4 (°/h)/Hz$^{1/2}$, which is negligible compared to the measured out-

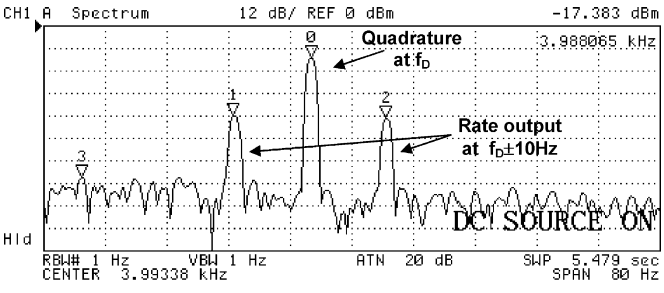

N	SWP PARAM	VAL
0	3.988065 kHz	-17.383 dBm
1	3.977995 kHz	-47.83 dBm
2	3.997762 kHz	-49.597 dBm
3	3.958228 kHz	-80.97 dBm

Fig. 10. The measured spectrum of the sense-mode output of the fabricated nickel angular rate sensor in response to a sinusoidal angular rate input of amplitude 2π °/s and frequency 10 Hz.

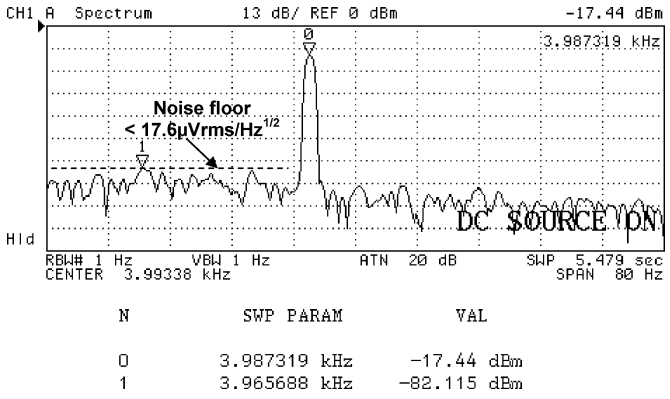

N	SWP PARAM	VAL
0	3.987319 kHz	-17.44 dBm
1	3.965688 kHz	-82.115 dBm

Fig. 11. The measured spectrum of the sense-mode output of the gyroscope when no angular rate input is applied to the gyroscope and the servo of the rate table is switched off.

put noise. The main source of the output noise is expected to be due to rotational mode of the fabricated nickel gyroscope, whose frequency approach to the operational frequency of the gyroscope during the fabrication due to the narrowed beam widths. The mechanical noise coupled to the sense-mode from the rotational mode would be suppressed in the future designs. The measured noise floor of the gyroscope corresponds to an rms-noise-equivalent rate of 0.11 (°/s)/Hz$^{1/2}$.

During rate measurements, it is observed that the servo of the rate table introduce significant noise if it is not switched off. Fig. 11 shows the measured spectrum of the sense-mode output of the gyroscope when no angular rate input is applied to the gyroscope and when the servo of the rate table is switched off. The rms noise floor of the gyroscope is found to be less than 17.6 μV/Hz$^{1/2}$, corresponding to the rms-noise-equivalent rate of 0.095 (°/s)/Hz$^{1/2}$, when the disturbance from the rate table is eliminated.

The sense-mode output of the gyroscope is demodulated, amplified through a 40 dB gain stage, and filtered by a low-pass network providing a dc output voltage proportional to the applied angular rate input. The output electronic blocks are currently constructed by off-the-shelf components, and they are intended for initial demonstration of gyroscope operation. Fig. 12 shows the measured output of angular rate sensor in response to rate inputs from 0 to −100 °/s and then to +100 °/s with 10 °/s steps. The sensor provides a reliable and repeatable output without any significant hysteresis. Fig. 13 shows the output response of the nickel gyroscope with respect to the applied angular rate input in a range from −100°/s to +100 °/s. The scale factor of the gyroscope is measured as 17.7 mV/(°/s), in agreement with the 180 μV peak sensitivity at the raw output of the capacitive interface circuit prior to demodulation and 40 dB amplification. The R^2-nonlinearity of the scale factor is only 0.12%, owing to the linear drive-mode vibrations and stress-relieving flexure design. The zero-rate output bias of the gyroscope is approximately 17 °/s, due to mechanical cross-talk between the drive and sense modes resulting from primitive phase-sensitive demodulation electronics. Only a 4° phase error would yield a zero-rate output offset of 17 °/s, for the measured quadrature signal of the fabricated gyroscope. The phase error introduced by the

Table 4
Look-up reference for checking the phase of the signals for the proposed gyroscope, depending on the frequency matching and the impedance of the interface circuit

Mode-matching	Interface type	X_{drive}	$V_{drive,out}$	Y_{sense}	$V_{sense,out}$
Matched	Capacitive	+90°[a]	+90°	±90°	±90°
	Resistive		In-phase		0° or 180°
Mismatched	Capacitive		+90°	0° or 180°	0° or 180°
	Resistive		In-phase		±90°

[a] Drive-mode is assumed to be at resonance during operation of the gyroscope.

analog-multiplier type demodulation stage limits the current performance of the gyroscope, and it can be reduced by using a balanced demodulator in the future designs.

Fig. 14 shows the random variation of the gyroscope output bias and the output noise measured for zero-rate input. The short-term (100 s) bias stability of the gyroscope is measured to be better than 0.1 °/s. The bias is observed to be stable within 1 °/s over 2 hours measurement period. The rms output noise of the sensor is measured to be 0.5 °/s in 30 Hz bandwidth, including noise contributions from the external signal processing electronics. The bandwidth of the angular rate sensor is set electronically by a low-pass filter and can be extended beyond 100 Hz, which will be then limited by the mechanical response bandwidth of the sense-mode of the gyroscope.

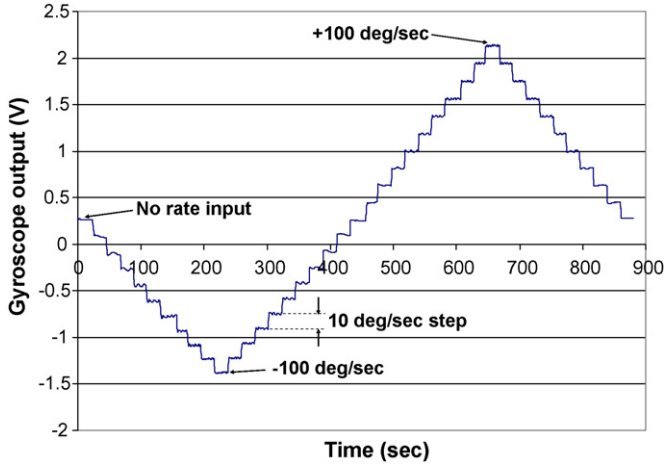

Fig. 12. The measured output of angular rate sensor in response to rate inputs from 0 to −100 °/s and then to +100 °/s with 10 °/s steps. The sensor provides a reliable and repeatable output without any significant hysteresis.

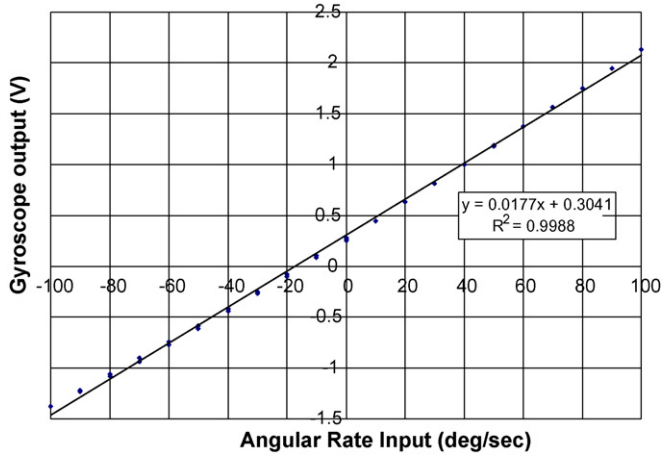

Fig. 13. The output response of the nickel gyroscope with respect to the applied angular rate input in a range from −100 °/s to +100 °/s. The scale factor of the gyroscope is measured as 17.7 mV/(°/s), in agreement with the 180 μV peak sensitivity at the raw output of the capacitive interface circuit prior to demodulation and 40 dB amplification. The R^2-nonlinearity of the scale factor is only 0.12%, owing to the linear drive-mode vibrations and stress-relieving flexure design.

The performance of the gyroscope is also evaluated at vacuum. Fig. 15 shows the resonance characteristics for the drive and sense modes of the fabricated gyroscope measured at 10 mTorr vacuum in a vacuum chamber. The quality factor of the drive-mode resonance reaches to 900 at vacuum, i.e., twice of the quality factor at the atmospheric pressure. This improvement helps decreasing the amplitude of the drive-mode actuation signal, and therefore, reducing the electrical cross-talk from the drive-mode to the sense-mode of the gyroscope. Similarly, the quality factor of the sense-mode resonance is measured to be 550 at vacuum, about an order of magnitude higher than the value measured at atmospheric pressure. The increase in the sense-mode quality factor at resonance reduces the mechanical noise from the gyroscope, improving the signal-to-noise ratio of the angular rate sensor. The improvement in the quality factor of the sense-mode yields an estimated noise-equivalent rate better than 0.05 (°/s)/$Hz^{1/2}$ in a narrowed response bandwidth of 10 Hz.

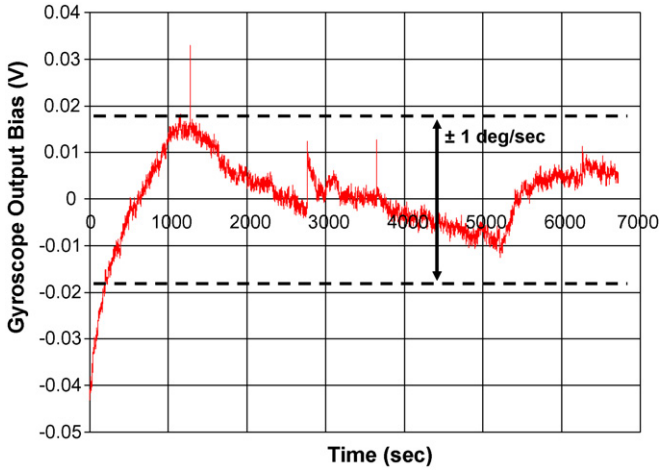

Fig. 14. The random variation of the gyroscope output bias and the output noise measured for zero-rate input. The short-term (100 s) bias stability of the gyroscope is measured to be better than 0.1 °/s. The bias is observed to be stable within 1 °/s over 2 hours measurement period. The rms output noise of the sensor is measured to be 0.5 °/s in 30 Hz bandwidth, including noise contributions from the external signal processing electronics.

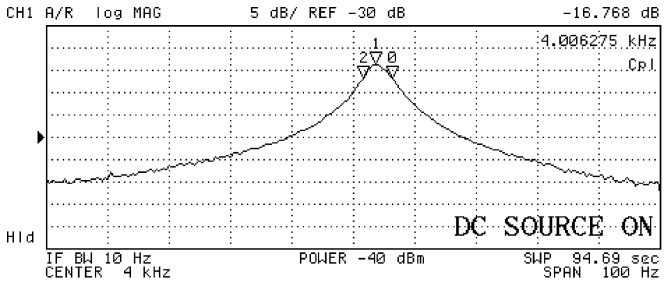

	N	SWP PARAM	VAL
	0	4.006275 kHz	−16.768 dB
	1	4.003725 kHz	−13.793 dB
(a)	2	4.001575 kHz	−16.794 dB

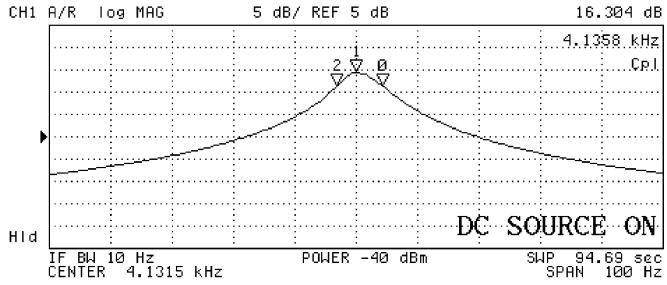

	N	SWP PARAM	VAL
	0	4.1358 kHz	16.304 dB
	1	4.1315 kHz	19.364 dB
(b)	2	4.128325 kHz	16.329 dB

Fig. 15. The resonance characteristics for (a) the drive and (b) the sense modes of the fabricated gyroscope measured at 10 mTorr vacuum. Quality factor of the drive and sense modes reach to 900 and 550, respectively.

Vacuum packaging of these gyroscopes is an important issue for commercialization. Wafer-level vacuum packaging approaches decrease the cost of the packaged gyroscopes [13], which are under consideration as a future work of this research.

5. Conclusions

In this paper, a low-cost microgyroscope with a resolution in the rate-grade at atmospheric pressure is presented. The gyroscope is fabricated through a simple nickel electroforming process, which is then hybrid connected to a custom made CMOS capacitive interface circuit. The mechanical structure is optimized for a small mechanical cross-talk with a high angular rate sensitivity. The fabricated gyroscope has a 18 μm-thick nickel structural layer with 2.5 μm capacitive gaps providing an aspect ratio above 7 and sensor capacitances about 0.5 pF. The resonance frequencies of the fabricated gyroscope are measured to be 4.09 kHz for the drive-mode and 4.33 kHz for the sense-mode, which are then matched by a tuning voltage less than 12 V dc. The fabricated rate sensor has a noise-equivalent rate of 0.095 (°/s)/$Hz^{1/2}$ at atmospheric pressure, a scale factor of 17.7 mV/(°/s), and an R^2-nonlinearity smaller than 0.12% in ±100 °/s measurement range. The short-term bias stability of the sensor is better than 0.1 °/s. The rms output noise of the sensor is measured to be 0.5 °/s in an electronically-set 30 Hz bandwidth. The quality factor of the sense-mode improves at vacuum by an order of magnitude, which yields an estimated noise-equivalent rate better than 0.05 (°/s)/$Hz^{1/2}$ in a narrowed response bandwidth of 10 Hz. The overall performance of the rate sensor satisfies rate-grade requirements both at atmospheric pressure and at vacuum. Wafer-level vacuum packaging approaches are under consideration as a future work of this research.

Acknowledgements

This research is sponsored by The Scientific and Technical Research Council of Turkey (TUBITAK-EEEAG 100E020) and The State Planning Organization (DPT) of Turkey. Authors would like to thank to Ilker Ender Ocak for his helps with fabrication and readout IC improvement and Kivanc Azgin for his helps in fabrication.

References

[1] F. Ayazi, K. Najafi, A HARPSS polysilicon vibrating ring gyroscope, J. Microelectromech. Syst. 10 (2) (2001) 169–179.
[2] S.E. Alper, T. Akin, A single-crystal silicon symmetrical and decoupled gyroscope on insulating substrate, in: Proceedings of the 12th International Conference on Solid-State Sensors and Actuators (Transducers '03), June 2003, pp. 1399–1402.
[3] K.Y. Park, H.S. Jeong, S. An, S.H. Shin, C.W. Lee, Lateral gyroscope suspended by two gimbals through high aspect ratio ICP etching, in: Proceedings of the 10th International Conference on Solid-State Sensors and Actuators (Transducers '99), June 1999, pp. 972–975.
[4] G. He, K. Najafi, A single-crystal silicon vibrating ring gyroscope, in: Proceedings of the IEEE Micro Electro Mechanical Systems Workshop (MEMS '02), Las Vegas, CA, January 2002, pp. 718–721.
[5] W. Geiger, W.U. Butt, A. Gaiβer, J. Frech, M. Braxmaier, T. Link, A. Kohne, P. Nommensen, H. Sandmaier, W. Lang, Decoupled microgyros and the design principle DAVED, Sens. Actuators A 95 (2002) 239–249.
[6] N. Hedenstierna, S. Habibi, S.M. Nilsen, T. Kvisteroy, G.U. Jensen, Bulk micromachined angular rate sensor based on the butterfly-gyro structure, in: Tech. Dig. IEEE Micro Electro Mechanical Systems Conference (MEMS '01), Interlaken, Switzerland, January 2001, pp. 178–181.
[7] H. Kawai, K.-I. Atsuchi, M. Tamura, K. Ohwada, High-resolution microgyroscope using vibratory motion adjustment technology, Sens. Actuators A 90 (1/2) (2001) 153–159.
[8] J.A. Geen, S.J. Sherman, J.F. Chang, S.R. Lewis, Single-chip surface micromachined integrated gyroscope with 50/spl deg//h Allan deviation, J. Solid State Cct. 37 (12) (2002) 1860–1866.
[9] S. Chang, M. Chia, P. Castillo-Borelley, W. Hidgon, Q. Jiang, J. Johnson, L. Obedier, M. Putty, Q. Shi, D. Sparks, S. Zarabadi, An electroformed CMOS integrated angular rate sensor, Sens. Actuators A 66 (1998) 138–143.
[10] S.E. Alper, K.M. Silay, T. Akin, A low-cost rate-grade nickel microgyroscope, in: Proceedings of the 19th European Conference on Solid-State Transducers (Eurosensors XIX), Barcelona, Spain, September 11–14, 2005.
[11] S.E. Alper, T. Akin, A symmetrical and decoupled nickel microgyroscope on insulating substrate, Sens. Actuators A 115 (2/3) (2004) 336–350.
[12] I.V. Kadija, A novel wet processing technology, in: Proceedings of the Symposium on High Rate Metal Dissolution Processes, vol. 95-19, The Electrochemical Society, 1995, pp. 1–14.
[13] www.saesgetters.com.

Biographies

Said Emre Alper was born in Ankara, Turkey, in 1976. He received the BS, MSc, and PhD degrees in electrical and electronics engineering with high honors from Middle East Technical University (METU) in Ankara, in 1998, 2000, and 2005, respectively. Between 1998 and 2005, he has worked as a research

assistant at METU in the Department of Electrical and Electronics Engineering, MEMS VLSI Research Group. Since 2006, he has been occupied as senior research scientist in the same department. His major research interests include capacitive inertial sensors, micromachined resonators and actuators, capacitive interface circuits, and microfabrication technologies. He is the first author of the symmetric and decoupled gyroscope design, which won the first prize award in the operational designs category of the "International Design Contest" organized by DATE and CMP in March 2001. He is also the first author of the tactical-grade symmetrical and decoupled microgyroscope design, which won the third prize award in the international "3-D MEMS Design Challenge" organized by MEMGEN Corporation (currently Microfabrica), in June 2003, among 132 MEMS designs from 24 countries and 25 states across United States.

Kanber Mithat Silay was born in Konya, Turkey, in 1982. He received the BS degree in electrical and electronics engineering with high honors from Middle East Technical University (METU), in Ankara, Turkey, in 2004. Currently, he is pursuing the MSc degree in electrical and electronics engineering at METU in the area of MEMS inertial sensors and their readouts. He has been working as a research and teaching assistant at METU in the Department of Electrical and Electronics Engineering since 2004. His research interests include MEMS capacitive inertial sensors, CMOS capacitive interface circuits, closed-loop control electronics for angular rate sensors, and analog and digital integrated circuit design.

Tayfun Akin was born in Van, Turkey, in 1966. He received the BS degree in electrical engineering with high honors from Middle East Technical University, Ankara, in 1987 and went to the USA in 1987 for his graduate studies with a graduate fellowship provided by NATO Science Scholarship Program through the Scientific and Technical Research Council of Turkey (TUBITAK). He received the MS degree in 1989 and the PhD degree in 1994 in electrical engineering, both from the University of Michigan, Ann Arbor. Since 1995, 1998, and 2004, he has been employed as an Assistant Professor, Associate Professor, and Professor, respectively, in the Department of Electrical and Electronics Engineering at Middle East Technical University, Ankara, Turkey. He is also the technical coordinator of METU-MET, an IC fabrication factory which is transferred to Middle East Technical University by the government for MEMS related production. His research interests include MEMS (Micro-Electro-Mechanical Systems), Microsystems Technologies, infrared detectors and readout circuits, silicon-based integrated sensors and transducers, and analog and digital integrated circuit design. He has served in various MEMS, EUROSENSORS, and TRANSDUCERS conferences as a Technical Program Committee Member. He is the co-chair of The 19th IEEE International Conference of Micro Electro Mechanical Systems (MEMS 2006) held in Istanbul. He is the winner of the First Prize in Experienced Analog/Digital Mixed-Signal Design Category at the 1994 Student VLSI Circuit Design Contest organized and sponsored by Mentor Graphics, Texas Instruments, Hewlett-Packard, Sun Microsystems, and Electronic Design Magazine. He is the co-author of the symmetric and decoupled gyroscope project which won the first prize award in the operational designs category of the international design contest organized by DATE Conference and CMP in March 2001. He is also the co-author of the gyroscope project which won the third prize award of 3-D MEMS Design Challenge organized by MEMGEN Corporation (currently, Microfabrica).